New Journal of Physics
The open–access journal for physics

Dimensionally constrained D'yakonov–Perel' spin relaxation in n-InGaAs channels: transition from 2D to 1D

A W Holleitner[1], V Sih[2], R C Myers[2], A C Gossard[2] and D D Awschalom[2,3]

[1] Department für Physik and Center for NanoScience (CeNS), Ludwig-Maximilians-University, 80539 Munich, Germany
[2] Center for Spintronics and Quantum Computation, University of California, Santa Barbara, CA 93106, USA
Email: awsch@physics.ucsb.edu

New Journal of Physics **9** (2007) 342
Received 30 March 2007
Published 28 September 2007
Online at http://www.njp.org/
doi:10.1088/1367-2630/9/9/342

Abstract. We investigate both the spin dynamics and the magnetotransport properties of two-dimensional (2D) n-InGaAs channels as a function of the channel width. We find that the electron spin scattering in the channels is limited by a dimensionally constrained D'yakonov–Perel' mechanism, while the magnetotransport reveals purely 2D behaviour. For submicron channels the spin relaxation times increase for decreasing widths, while the magnetotransport data exhibit no band bending effects for the investigated samples. Temperature and photon energy dependent measurements rule out dissipative effects and further corroborate the experimental observation of a dimensionally constrained spin relaxation.

Semiconductor spintronics seeks extra functionality compared with conventional electronics by exploiting the carrier spin degree of freedom [1]–[4]. For a potential information processing scheme which combines quantum mechanical and classical data, it is of particular interest to manipulate and to control carrier spin dynamics in non-magnetic materials by utilizing the spin–orbit interaction [5]–[8]. In three- and two-dimensional (3D and 2D) carrier systems, spin–orbit coupling creates a randomizing momentum-dependent effective magnetic field; the corresponding relaxation process is known as the D'yakonov–Perel' (DP) mechanism [9]. In an ideal 1D system, a complete suppression of the DP spin relaxation has been predicted,

[3] Author to whom any correspondence should be addressed.

PII: S1367-2630(07)47415-8

if the lateral width of a 2D channel is reduced to be on the order of the electron mean free path [10]–[13]. The predictions are made for semiconductor heterostructures, such as InGaAs quantum wells, in which the spin–orbit interactions are dominated by structural inversion asymmetry (SIA) [14]–[19]. Such solid-state systems have been proposed as candidates for spintronic devices, including spin transistors [7], due to their potential scalability and compatibility with existing semiconductor technology [20]–[23]. For the regime approaching the 1D limit, we recently reported a progressive slowing of the spin relaxation in InGaAs channels, which is in agreement with a dimensionally constrained DP mechanism [24]. A similar dimensional crossover has been observed by means of a weak antilocalization analysis of magnetotransport studies on InAs channels [25]. The dimensional crossover can be understood in terms of an interplay between the channel width, the spin precession length over which the electrons remain spin polarized [26, 27], and the effect of spin scattering at the boundaries of the channels [28].

Here, we present additional magnetotransport measurements on the same 2D, n-doped InGaAs quantum well channels previously measured. The magnetotransport measurements reveal that the electron gases can be considered to be 2D for channel widths w larger than 500 nm, while the time-resolved Faraday rotation (TRFR) data on the spin dynamics can be understood in terms of a dimensionally constrained DP mechanism for $w < 5\,\mu$m. Temperature and photon energy dependent measurements demonstrate that energy dissipative effects play only a minor role to the spin dynamics in the channels. We further find that channels along the crystallographic directions [100] and [010] show longer spin relaxation times than channels along [110] and [−110]. We interpret the anisotropy such that the cubic spin-orbit coupling terms due to bulk inversion asymmetry (BIA) start to dominate the spin relaxation in the narrowest channels [27], [29]–[32]. For the narrowest channels, the spin relaxation process due to the Elliott–Yafet (EY) mechanism becomes important due to increased impurity scattering [33].

The spin splitting in a 2D quantum well due to SIA can be expressed in the form of an effective angular frequency vector as

$$\boldsymbol{\Omega}(\boldsymbol{k}) = (1/l_{\mathrm{SP}})[\boldsymbol{v}(\boldsymbol{k}) \times \hat{z}], \tag{1}$$

with $\boldsymbol{k}$ the momentum vector and $\boldsymbol{v}(\boldsymbol{k})$ the velocity of an electron [3]. $\hat{z}$ is the unit vector perpendicular to the quantum well, and l_{SP} is the spin precession length, over which the electrons remain spin polarized. In the case of motional narrowing [34], the corresponding spin relaxation rate can be described as

$$\tau_{\mathrm{SP}}^{-1} = |\boldsymbol{\Omega}(\boldsymbol{k})|^2\, \tau_{\mathrm{M}}/2, \tag{2}$$

with τ_{M} the momentum scattering time. Given a system with a fixed mean free path, a larger effective angular frequency induces faster spin rotations and, in turn, a shorter spin relaxation time. Figure 1(a) depicts the orientation of the spin eigenfunctions for two spin-split subbands E_+ and E_- of a zincblende quantum well in the presence of SIA (E_+ and E_- are defined as in [29]). For SIA, the spin eigenfunctions are always oriented perpendicular to $\boldsymbol{k}$, and in turn, a constant value of $|\boldsymbol{\Omega}(\boldsymbol{k})|$ is expected that only depends on the magnitude of $\boldsymbol{k}$. Figure 1(b) shows the orientation for the spin eigenfunctions in the case of BIA. Here, both the direction of the spin eigenfunctions and the absolute value of $|\boldsymbol{\Omega}(\boldsymbol{k})|$ depend significantly on the vector $\boldsymbol{k}$ [29]. The directions along [100] and [010] show similar behaviour, distinct from the directions [110] and [−110]. Therefore, we expect a $\boldsymbol{k}$-vector anisotropy in spin systems where the DP spin relaxation due to BIA dominates the spin relaxation [35]. In particular, linear-in-$\boldsymbol{k}$ terms due to pure BIA

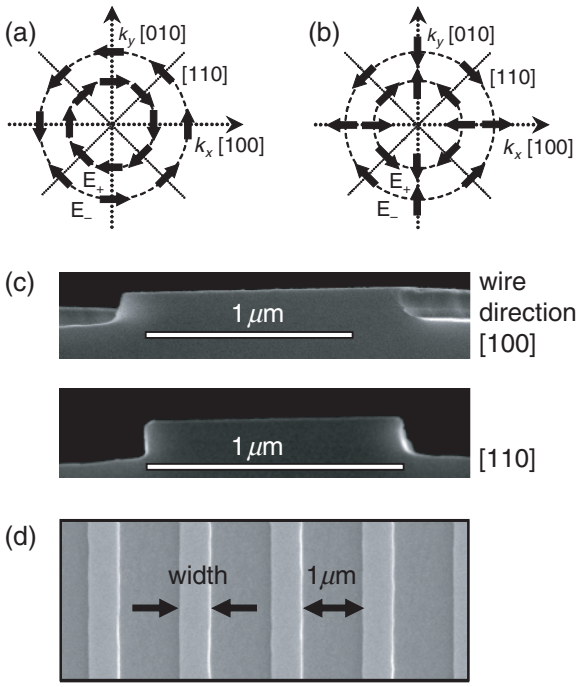

Figure 1. Schematic vector map of the spin eigenfunctions in a quantum well with (a) SIA and (b) BIA. (c) Scanning electron micrograph of sample A along the [−110] cleaving direction. Both channels along [100] and [110] have a width of $(1.02 \pm 0.04)\,\mu$m. (d) Scanning electron micrograph of dry-etched InGaAs channels, which are patterned along the four crystallographic directions [100], [110], [010] and [−110]. The channel widths are varied between 420 nm and 20 μm, while their separation is fixed at 1 μm. The figure is partly adapted from [24].

shown in figure 1 result in an anisotropy of direction of the effective angular frequency vector but its strength remains isotropic. The anisotropy of the effective angular frequency vector due to $\boldsymbol{k}$-linear terms, and, consequently, of DP relaxation for spins oriented normal to the QW plane, may be caused by the interference of BIA and SIA i.e. for BIA∼SIA [35]. The cubic in $\boldsymbol{k}$ BIA terms are essentially anisotropic and should result in the anisotropy of DP spin relaxation in the case of dominating BIA. The cubic in $\boldsymbol{k}$ terms vanish for [100]- and [010]-directions and the DP spin relaxation time increases.

In order to probe the spin dynamics for different electron $\boldsymbol{k}$-vectors, magnetotransport and spin coherence experiments are performed on a set of n-doped InGaAs channels (see figures 1(c) and (d)). The channels are patterned along the crystallographic directions [100], [110], [010] and [−110], while the spins are optically oriented along the growth direction [001]. Structures are fabricated by e-beam lithography and reactive ion etching out of three modulation-doped n-$In_{0.2}Ga_{0.8}As$/GaAs quantum wells, the same as used in [24]. The unpatterned quantum wells A, B and C have the following sheet densities n_S and mobilities at a temperature of $T = 5$ K: (A) 5.4×10^{11} cm^{-2} and 3.8×10^4 cm^2 (V s)$^{-1}$, (B) 6.6×10^{11} cm^{-2} and 3.1×10^4 cm^2 (V s)$^{-1}$, and (C) 7.0×10^{11} cm^{-2} and 2.4×10^4 cm^2 (V s)$^{-1}$ [24], [36]. The quantum wells are situated 100 nm below the surface of the heterostructures, and the quantum well width is $\Delta z = 7.5$ nm.

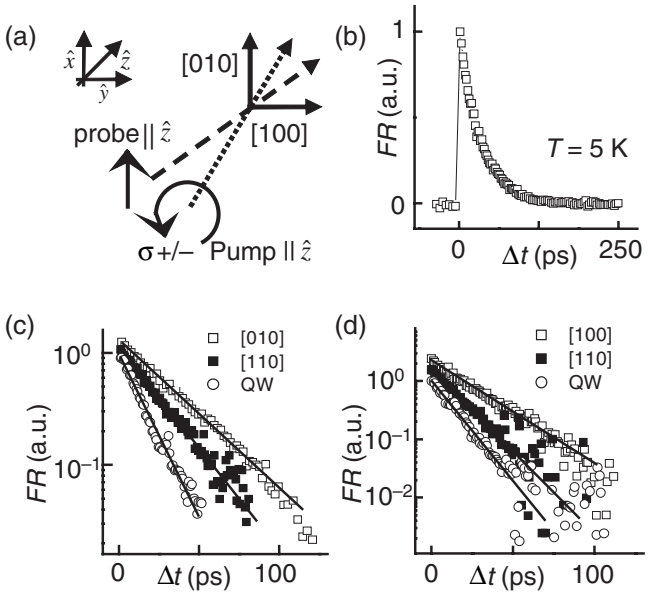

Figure 2. (a) TRFR: a circularly-polarized pump pulse excites spin carriers in the channels, while a time-delayed linearly-polarized probe pulse detects the orientation of the spins. (b) TRFR signal of channels with a width of 750 nm-channels patterned along [010] on sample A at zero magnetic field. (c) TRFR at 5 K for sample A (open circles) and 750 nm channels patterned along [010] (open squares) and [110] (filled squares) in logarithmic scale. (d) Similar TRFR data at 5 K for sample B (open circles) and 750 nm channels patterned along [100] (open squares) and [110] (filled squares). Black lines are guides to the eye, and the data are off-set for clarity. The figure is partly adapted from [24].

The widths of the channels w range between 420 nm and 20 μm, and the height of the channels is chosen to be 150 nm. After patterning, n_S is reduced by about (17 ± 1) %, and the mobility is lowered by about (5 ± 5) %. The magnetotransport experiments are performed on single channels (figure 1(c)). For the optical experiments, the channels are arranged in arrays with the dimension of $200 \times 200\,\mu\text{m}^2$ (figure 1(d)), while the diameter of the laser spot is about 50 μm. In order to provide constant etching parameters for all widths and directions of the channels, the distance between adjacent channels is set to be 1 μm for all of the arrays. Generally, we utilize InGaAs quantum wells with a relatively low indium concentration. The corresponding spin precession length $l_{SP} \cong (0.9 - 1.1)\,\mu$m yields a Rashba spin coupling constant of $\alpha \equiv \hbar^2/(2l_{SP}m^*) \cong (0.5 - 0.7) \times 10^{-12}$ eVm (with m^* the effective electron mass in the InGaAs quantum wells) [3, 12, 24]. These values are in good agreement with previous results on InGaAs quantum wells [15]. Most importantly, the set of parameters ensures that the spin precession length is in the range of the channel widths of the samples, and that the quantum wells are in the 'motional narrowing' regime. Both are important preconditions to detect the dimensionally-constrained DP mechanism in submicron channels as presented here [10]–[13], [27, 28].

As sketched in figure 2(a), the electron spin dynamics are probed with the TRFR technique, using 150 fs pulse trains from a mode-locked Ti:sapphire laser tuned to the absorption edge of the

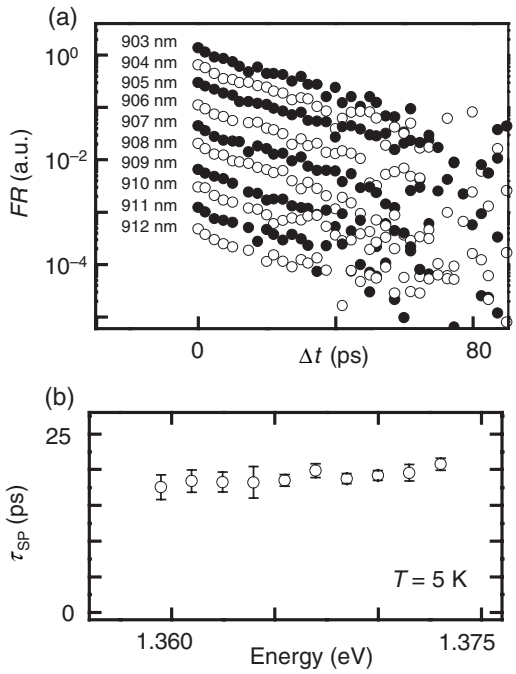

Figure 3. (a) Energy dependence of the TRFR signal for channels formed in sample B with a width of 1.25 μm and a direction along [100] at 5 K. The Faraday rotation signal can be fitted to a single exponential decay curve; here for a wavelength range between 903 and 912 nm. (b) Spin relaxation time deduced from the data in (a) as a function of the photon energy.

quantum wells (e.g. $E_{\mathrm{LASER}} = 1.37$ eV for sample B). To this end, a circularly-polarized pump pulse excites the spin polarization in the channels, while a linearly-polarized probe pulse detects the spin dynamics as a function of the time-delay Δt between both laser pulses. A typical TRFR curve is depicted in figure 2(b) for channels with a width of 750 nm patterned on sample A. The evolution of the Faraday rotation angle can be described by a single exponential decay $\theta_{\mathrm{F}} = A_1 \mathrm{e}^{-\Delta t/\tau_{\mathrm{SP}}}$, where A_1 and τ_{SP} are the amplitude and the relaxation time of the electron-spin polarization. In figures 2(c) and (d), TRFR data are presented for sample A (B) in the case of the unpatterned quantum well (open circles) and channels. The channels have a width of 750 nm and crystallographic directions along [010] and [110] (open and filled squares in (c)) and [100] and [110] (open and filled squares in (d)). As shown with solid lines, the exponential behaviour of the data is described by a single longitudinal spin relaxation time τ_{SP} for both the unpatterned quantum well and for the channels aligned along different crystallographic directions. The fact that the data scale to exponential curves suggests that a single spin species is observed, i.e. electron spins and not hole spins.

In principle, the TRFR-technique is sensitive to a variation of the spin relaxation times at $E_{\mathrm{LASER}} \sim 1.36$ eV, since the upper limit of the full-width at half-maximum of the laser is about 12 meV (for 150 fs pulses). As a function of the photon energy, figure 3(a) depicts data taken for channels processed on sample B with a width of 1.25 μm and a crystallographic direction of [010]. We find a single exponential decay curve for all photon energies. In figure 3(a) the photon energy is varied in the range of 1.358 eV $< E_{\mathrm{LASER}} <$ 1.372 eV (912 nm $> \lambda_{\mathrm{LASER}} >$ 903 nm), while the

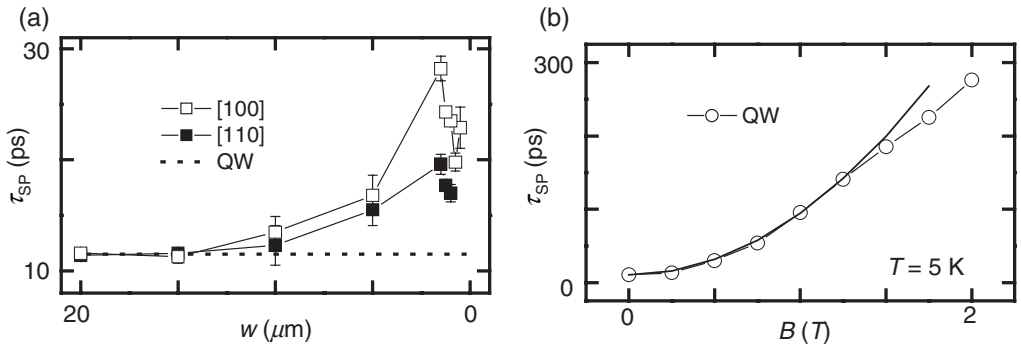

Figure 4. (a) Width dependence of spin relaxation times for channels fabricated from sample C. Open and filled squares represent data of channels along [100] and [110], while the dotted line depicts the spin relaxation time of the unstructured quantum well. (b) Magnetic field dependence of spin relaxation times in the unprocessed sample. The magnetic field is applied perpendicular to the surface of the sample. The figure is partly adapted from [24].

absorption edge and the Fermi energy of sample B are $E \sim 1.36\,\text{eV}$ and $E_{\text{FERMI}} = 22\,\text{meV}$. As can be seen in figure 3(b), the spin relaxation time varies only slightly throughout the range of photon energies investigated. We conclude from figure 3 that the optically measured spin relaxation time coincides with the electron spin relaxation time at the Fermi energy of the quantum wells within a certain experimental error. Most importantly, the present variation in spin relaxation time is less than the increase of the spin lifetime which we find for narrow channels as presented below in figure 4(a).

Figure 4(a) presents the major result of the paper: for all samples and widths narrower than $\sim 10\,\mu\text{m}$, the spin relaxation times in the channels are longer than in the unpatterned quantum wells. In addition, we find that channels aligned along [100] and [010] show equivalent spin relaxation times, which are generally longer than the spin relaxation times of channels patterned along [110] and [−110] (for clarity, only the data for the directions [100] and [110] are shown). The observations can already be seen in the original data of figures 2(c) and (d). In order to demonstrate that the increase of the spin relaxation time is due to a dimensionally constrained DP mechanism, we first verify that the spin dynamics in the measured structures is dominated by the DP mechanism. Generally, the precession axis of the electron spin can be fixed independently of the scattered momentum vector, if an external magnetic field is applied. In the case that the DP mechanism is the dominant relaxation process, the following magnetic field dependence of the spin relaxation time has been predicted (for $\omega_C \tau < 1$) [37]:

$$\tau_{SP}(B) = \tau_{SP}(0)[1 + (\omega_C \tau)^2], \tag{3}$$

where $\omega_C = eB/m^*$ is the cyclotron frequency of an electron with charge e, $m^* = 0.064\,m_e$ is the effective electron mass [36], and τ represents the intrinsic electron scattering time. The magnetic field dependence of the spin relaxation time for the unpatterned quantum wells is well fit by this prediction (for $B < 1.25\,\text{T}$ in figure 4(b)). We find $\tau \sim 1\,\text{ps}$, in agreement with the measured momentum scattering time τ_M in these quantum wells. In contrast, the EY mechanism should not exhibit this dependence on magnetic field. As a result, the spin dynamics of the samples can

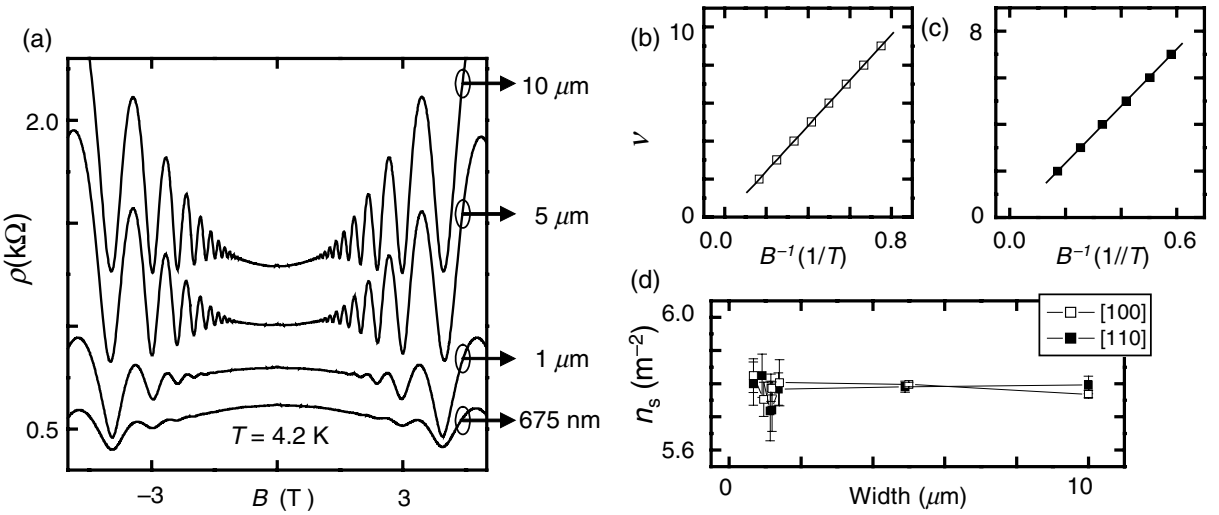

Figure 5. (a) Magnetoresistance for individual channels of sample C with a width of 10 μm, 5 μm, 1 μm, and 675 nm oriented along [110] at 4.2 K. The data are off-set for clarity. (b) and (c) Landau filling factors as function of the inverse magnetic flux measured for individual channels. The graph in (b) represents a channel with a width 5 μm and an orientation along [100] and (c) depicts data of a channel with a width 675 nm and an orientation [110]. (d) Sheet density of the channels as a function of the channel width.

be described by equation (2), which is the DP mechanism (the magnetic field dependent data for the channel is not shown).

To examine the 2D character of the electron gases, magnetotransport measurements are performed on single channels in a four point geometry at 4.2 K. Figure 5(a) depicts the corresponding magnetotransport data for single channels patterned on sample C. For all channel widths and directions, we detect Shubnikov–de Haas oscillations, which are characteristic of the 2D electron systems in the quantum wells. In figures 5(b) and (c), the Landau filling factors of the 2D electron gases are plotted versus the inverse of the applied magnetic flux for two different channels. Such fan diagrams give a sensitive measure of band bending at the boundaries of the InGaAs channels. Only a deviation from a linear dependence for large filling factors would indicate that the band bending at the boundaries of the channels influences the 2D electron dynamics [38]. However, we find that band bending effects are absent for any channel with a width larger than ~500 nm. Furthermore, the 2D electron density n_S in the channels is deduced from the linear regression lines in figures 5(b) and (c), since the slope of the fan diagrams is given by $n_S h/e$, with h Planck's constant. Within the experimental error the 2D electron density n_S in the channels shows no dependence on the channel width and direction down to about $w \sim 500$ nm (figure 5(d)). The latter observation suggests that the spin relaxation mechanism proposed by Bir *et al* [39] which depends on the carrier density, is only of minor importance to the spin dynamics in the InGaAs channels.

The magnetotransport data also give insight into the intrinsic scattering times in a 2D electron system: namely, the momentum scattering time and the electron quantum lifetime. The momentum scattering time τ_M is given by the conductivity σ at zero magnetic field via $\sigma = n_S \tau_M e^2/m^*$, where n_S is the electron density of the electron gas and e the electron charge.

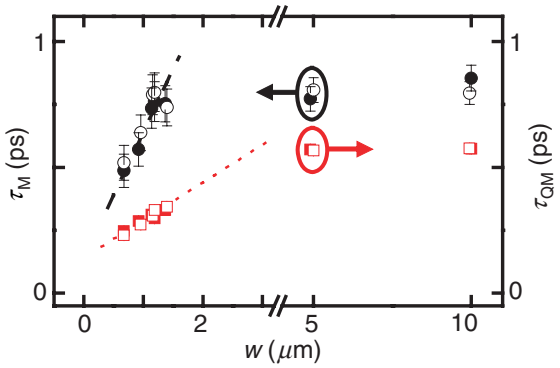

Figure 6. Momentum scattering time (circles) and quantum lifetime (squares) versus channel width for the directions [100] (open symbols) and [110] (filled symbols), respectively. The dotted lines are guides to the eye. The figure is partly adapted from [24].

An estimate of the quantum lifetime τ_{QM} is gained by plotting the Shubnikov–de Haas oscillations in a Dingle plot (data not shown) [40]. The ratio between the momentum scattering time and the quantum lifetime gives a measure for the relative contribution of the large and small angle scattering mechanisms [41]. Figure 6 shows the dependence of τ_M and τ_{QM} on the channel width. Both scattering times show a rapid decrease for the narrowest channels. We would like to note a few points. Since the spin relaxation times greatly exceed the charge scattering times, the quantum wells can be considered to be in the 'motional narrowing' regime, and in turn, equation (2) can be assumed to be valid [34]. Figure 6 further demonstrates that τ_M is constant for channels with $w \geqslant 1.2\,\mu$m, independent of the crystallographic direction (the value of the momentum scattering time corresponds to a mean free path $l_e = (275 \pm 5)$ nm). In figure 4(a), we find an enhanced spin coherence for channels with $w \leqslant 5\,\mu$m. The combination of both results implies that for $1.2\,\mu\text{m} \leqslant w \leqslant 5\,\mu$m the effective angular frequency $|\boldsymbol{\Omega}(\boldsymbol{k})|$ is reduced, according to equation (2). Such a slowing of the spin relaxation is a precursor of the dimensionally constrained DP mechanism [10]–[13], [27, 28]. In principle, a greater inversion asymmetry may be introduced by the edges in the in-plane direction perpendicular to the channels; an effect which should be detectable especially for the narrowest channels. The Fermi wavelength in the channels would be the relevant length scale for such an effect. However, the Fermi wavelength of the channels $\lambda_F = 30$–35 nm is a factor of about twenty times smaller than the narrowest channel widths. At the same time, a greater inversion asymmetry induced at the channel edges should give shorter spin relaxation times. Our results for $1.2\,\mu\text{m} \leqslant w \leqslant 5\,\mu$m show longer spin relaxation times for a decreasing channel width. Hereby, we assume that band bending effects at the boundaries of the channels are negligible for $w \geqslant 1.2\,\mu$m; the range of widths where we draw our main conclusions. In addition, for micron sized channels the magnetotransport data show that the electron systems are still 2D (figure 5).

Recently, we reported that the quantum lifetime τ_{QM} (as in figure 6) correlates to the DP spin relaxation time in narrow channels for $w < 10\,\mu$m [24]. The observation is in agreement with measurements by Brand *et al* [42]. which demonstrated that in the 'motional narrowing regime' the electron scattering time which correlates to the spin relaxation time via equation (2) is shorter than the momentum scattering time. Brand *et al* further showed that a decrease of the scattering time due to heating results in an increase of the spin relaxation time [42]. However,

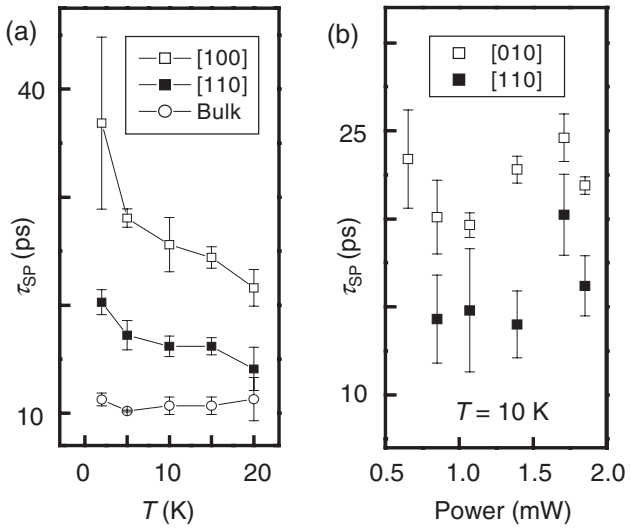

Figure 7. (a) Temperature dependence of the spin relaxation time for channels formed in sample C with a width of 1.5 μm. Open and filled squares represent data of channels along [100] and [110], while the open circles depict the spin relaxation time of the unstructured quantum well. (b) Pump power dependence for channels formed in sample A with a width of 750 nm at 10 K.

we can exclude such dissipation effects in the channels, since the data in figure 7(a) for sample C demonstrates that a temperature rise results in a decrease of the spin relaxation time in the channels. In addition, our conclusions about a dimensionally constrained DP mechanism are drawn in the case that the momentum scattering time and the quantum lifetime are constant as a function of the channel width ($1.2\,\mu m < w < 5\,\mu$m).

Generally, the optical measurements are performed at low excitation power. Typical values of the excitation power are 400 μW for the pump pulse and 60 μW for the probe pulse. At least 40% of the pump pulse is transmitted and not absorbed within the samples, since the photon energy $E_{\mathrm{LASER}} \sim (1.3\text{–}1.4)$ eV is much smaller than the band gap of the GaAs substrates $E_{\mathrm{GaAs}} = 1.52$ eV. Figure 7(b) presents the spin relaxation times as a function of the pump power for channels with $w = 750$ nm patterned on sample A at $T = 10$ K. We find that the variation of the spin lifetime, which is due to a varying power, is less than the difference between the spin lifetime of channels patterned along [100] ([110]) and [110] ([−110]) (the spin relaxation time for the unpatterned quantum well is $\tau_{\mathrm{SP}} = (13.3 \pm 1.3)$ ps). This result further corrobates the interpretation that the spin relaxation mechanism proposed by Bir *et al* [39] is only of minor importance to the spin dynamics in the InGaAs channels.

We calculated the energy dispersion for an InGaAs quantum well along in-plane $\boldsymbol{k}$-vectors [100] and [110] in an 8 × 8 k.p perturbation theory model with parameters which refer to sample A[4]. All samples exhibit typical Fermi-wavevectors of about 0.018 to 0.021 Å^{-1}. Figure 8(a) demonstrates that for such $\boldsymbol{k}$-vectors the energy dispersion is rather isotropic for the electron state e1, and the first two hole states h1 and h2 of the quantum well. Only for $|\mathrm{k}| > 0.025\,1$ Å^{-1} does the energy dispersion start to be anisotropic. In the magnetotransport measurements we find that the electron density of channels larger than 675 nm is constant within

[4] For the simulations the software package of nextnano3 is used, online at http://www.nextnano.de

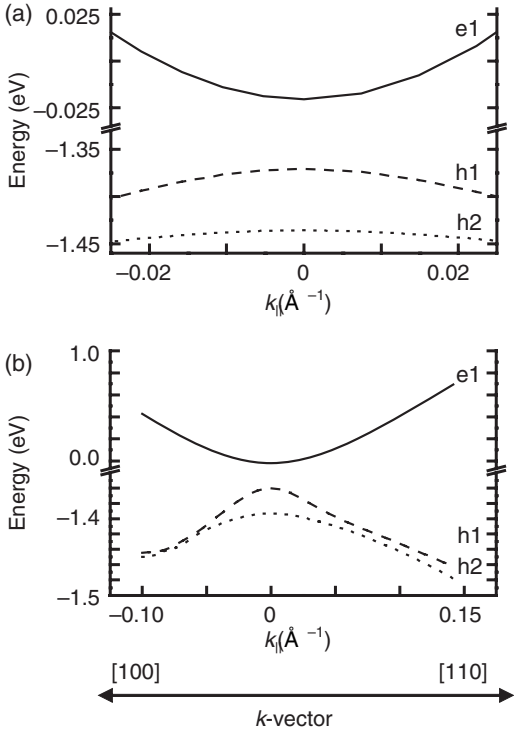

Figure 8. Energy of the electron state e1 and the hole states h1 and h2 in the quantum well as a function of the in-plane $k_{\|}$-vector for a strained $In_{0.2}Ga_{0.8}As$ QW. The data are results of a 8×8 k.p simulation for a temperature of 5 K [43]. (a) For $|k_{\|}| < 0.025$ the energy dispersion is similar for directions [100] and [110]. (b) Only for larger in-plane vectors does the energy dispersion become anisotropic.

the experimental error. Therefore, the Fermi-wavevectors can be assumed to be constant for all channel widths which are relevant for the main conclusion of the paper ($1.2\,\mu m \leqslant w \leqslant 5\,\mu m$). As a consequence from the k.p simulation and the transport data, the g-factor can be assumed to vary only negligibly for all channel widths and directions. In addition, the Fermi-wavelength is rather small compared to the channel width. Therefore, we assume that the effect of the channel width on the Lande g-factor can be neglected. Most importantly, all conclusions of the paper are drawn for the case that no external magnetic field is applied. Therefore, the Zeeman splitting is zero. Only figure 4(b) of the paper depicts data taken at a finite magnetic field, in order to demonstrate that the DP mechanism is the dominant spin relaxation mechanism in the 2D channels at zero field.

So far, we have demonstrated that the increase of the spin relaxation time in the InGaAs channels for decreasing widths can be understood as a dimensionally constrained DP mechanism, while the electron dynamics are still 2D as far as the magnetotransport is concerned. We further have shown that the anisotropy between channels patterned along [100] ([010]) and [110] ([−110]) cannot be explained by the discussed effects as hitherto. We observe from the images shown in figure 1(c) that the channels are homogeneously etched. Consequently, strain relaxation in the quantum wells via dislocation nucleation is unlikely for channels with $1.2\,\mu m \leqslant w \leqslant 5\,\mu m$ and a quantum well width of $\Delta z = 7.5$ nm [43]. However, an anisotropy in the spin-splitting

and, thus, in $|\boldsymbol{\Omega}(\boldsymbol{k})|$ has been predicted for InGaAs quantum wells assuming cubic BIA terms and Fermi-wavevectors which are comparable to $k_F = \sqrt{2\pi\, n_S} \cong (0.018 - 0.021)\,\mathrm{A}^{-1}$ of the discussed samples [29]. Since the spin-splitting due to BIA is anisotropic and since it can even vanish for cubic in $\boldsymbol{k}$ BIA terms along the directions [100] and [010] (figure 1(b)), the magnitude of $|\boldsymbol{\Omega}(\boldsymbol{k})|$ depends sensitively on the momentum vector. Given a constant scattering time and equation (2), this anisotropy can explain why spin lifetimes are similar for channels oriented along [100] and [010], but are different for channels patterned along the [110] and [−110] directions. In such narrow 2D electron systems the DP spin relaxation, which is caused by $\boldsymbol{k}$-linear terms due to BIA and SIA, is suppressed by a dimensionally constrained DP mechanism, while the cubic in $\boldsymbol{k}$ terms still influence the DP spin relaxation. Since the cubic in $\boldsymbol{k}$ terms can even vanish for [100]- and [010]-directions, the DP spin relaxation time in channels along these directions is longer than for channels along the [110] and the [−110] direction. We would like to note that the temperature dependence of the spin relaxation time as presented in figure 7(a) is in agreement with the interpretation that the cubic in $\boldsymbol{k}$ terms of the BIA dominate the spin dynamics in the narrowest channels. In figure 7(a) we find that the difference in spin relaxation times for channels along [100] and [110] decrease for an increasing temperature; a result which has been recently predicted by reason of electron–electron and electron–phonon scattering [35]. For the narrowest channels, the spin relaxation mechanism proposed by Elliot and Yafet [33] is likely to be present, since scattering processes at impurities eventually dominate the charge carrier dynamics.

In summary, an effective slowing of the DP spin relaxation mechanism is observed in unexpectedly wide n-InGaAs quantum channels. The magnetotransport data demonstrate that the electron systems can be considered to be 2D. The results on the spin dynamics are consistent with a dimensionally-constrained DP mechanism as recently predicted for narrow 2D quantum wells exhibiting SIA. For the narrowest channels, the spin relaxation due to the cubic terms of the BIA dominates the spin relaxation.

Acknowledgments

We thank Y Li and S Birner for technical support and F Meier for stimulating discussions. We gratefully acknowledge financial support by the AFOSR, NSR, ONR, DARPA, project DFG-HO 3324/4 and the Center for NanoScience (CeNS) in Munich and the German excellence initiative via the cluster ‘Nanosystems Initiative Munich (NIM)’.

References

[1] Prinz G A 1998 *Science* **282** 1660
[2] Wolf S A, Awschalom D D, Buhrman R A, Daughton J M, von Molnar S, Roukes M L, Chtchelkanova A Y and Treger D M 2001 *Science* **294** 1488
[3] Awschalom DA, Loss D and Samarth N 2002 *Semiconductor Spintronics and Quantum Computation* (Berlin: Springer)
[4] Awschalom D D and Flatte M E 2007 *Nature Phys.* **3** 153
[5] Lommer G, Malcher F and Rössler U 1988 *Phys. Rev. Lett.* **60** 728
[6] Luo J, Munekata H, Fang F F and Stiles P J 1988 *Phys. Rev.* B **38** 10142
[7] Datta S and Das B 1990 *Appl. Phys. Lett.* **56** 665
[8] Kato Y, Myers R C, Gossard A C and Awschalom D D 2004 *Nature* **427** 50

[9] D'yakonov M I and Perel' V I 1971 *Zh. Eksp. Teor Fiz.* **60** 1954
D'yakonov M I and Perel' V I 1971 *Sov. Phys.—JETP* **33** 1053 (Engl. Transl.)
D'yakonov M I and Kachorovskii V Y 1986 *Fiz. Techn. Poluprov* **20** 178
D'yakonov M I and Kachorovskii V Y 1986 *Sov. Phys.-Semicond.* **20** 110
[10] Bournel A, Dollfus P, Bruno P and Hesto P 1998 *Eur. Phys. J. Appl. Phys* **4** 1
[11] Mal'shukov G and Chao K A 2000 *Phys. Rev.* B **61** 2413
[12] Kiselev A and Kim K W 2000 *Phys. Rev.* B **61** 13115
[13] Pareek T P and Bruno P 2002 *Phys. Rev.* B **65** 241305
[14] Nitta J, Akazaki T, Takayanagi H and Enoki T 1997 *Phys. Rev. Lett.* **78** 1335
[15] Koga T, Nitta J, Akazaki T and Takayanagi H 2002 *Phys. Rev. Lett.* **89** 046801
[16] Grundler D 2000 *Phys. Rev. Lett.* **84** 6074
[17] Ganichev S D 2004 *Phys. Rev. Lett.* **92** 256601
[18] Miller J B, Zumbauhl D M, Marcus C M, Lyanda-Geller Y B, Goldhaber-Gordon D, Campman K and Gossard A C 2003 *Phys. Rev. Lett.* **90** 076807
[19] Averkiev N S and Golub L E 1999 *Phys. Rev.* B **60** 15582
[20] Schäpers T, Knobbe J and Guzenko V A 2004 *Phys. Rev.* B **69** 235323
[21] Hansen A E, Bjrk T M, Fasth C, Thelander C and Samuelson L 2005 *Phys. Rev.* B **71** 205328
[22] Schliemann J, Egues J C and Loss D 2003 *Phys. Rev. Lett.* **90** 146801
[23] Heida J P, van Wees B J, Kuipers J J, Klapwijk T M and Borghs G 1998 *Phys. Rev.* B **57** 11911
[24] Holleitner A W, Sih V, Myers R C, Gossard A C and Awschalom D D 2006 *Phys. Rev. Lett.* **97** 036805
[25] Wirthmann A, Gui Y S, Zehnder C, Heitmann D, Hu C M and Kettemann S 2006 *Physica* E **34** 493
[26] Dragomirova R L and Nikolic B K 2006 *Preprint* cond-mat/0604187
[27] Kettemann S 2006 *Preprint* cond-mat/0605243
[28] Schwab P, Dzierzawa M, Gorini C and Raimondi R 2006 *Phys. Rev.* B **74** 155316
[29] Winkler R 2004 *Phys. Rev.* B **69** 045317
[30] Ting D Z Y and Cartoixa X 2003 *Phys. Rev.* B **68** 235320
[31] Lusakowski A, Wrobel J and Dietl T 2003 *Phys. Rev.* B **68** 081201
[32] Liu M H, Chang C R and Chen S H 2005 *Phys. Rev.* B **71** 153305
[33] Elliott R J 1954 *Phys. Rev.* **96** 266
Yafet Y 1963 *Solid State Physics* vol 13, ed F Seitz and D Turnbull (New York: Academic)
[34] Lau W H, Olesberg J T and Flatté M E 2001 *Phys. Rev.* B **64** 161301
[35] Jiang L and Wu M W 2005 *Phys. Rev.* B **72** 033311
[36] Sih V, Lau W H, Myers R C, Gossard A C, Flatté M E and Awschalom D D 2004 *Phys. Rev.* B **70** 161313
[37] Meier F and Zakharchenya B P 1984 *Optical Orientation* (Amsterdam: Elsevier)
[38] Berggren K F, Roos G and van Houten H 1988 *Phys. Rev.* B **37** 10118
[39] Bir G L, Aronov A G and Pikus G E 1975 *Zh. Eksp. Teor. Fiz.* **69** 1382
[40] Dingle R B 1952 *Proc. R. Soc.* A **211** 517
[41] Das Sarma S and Stern F 1985 *Phys. Rev.* B **32** 8442
[42] Brand M A *et al* 2002 *Phys. Rev. Lett.* **89** 236601
[43] Knotz H, Holleitner A W, Stephens J, Myers R C and Awschalom D D 2006 *Appl. Phys. Lett.* **88** 241918